焊接机器人再制造中结构光传感器的标定

殷子强， 张广军， 高洪明， 吴 林
（哈尔滨工业大学 现代焊接生产技术国家重点实验室，哈尔滨 150001）

殷子强

摘 要：在基于焊接机器人的柔性再制造平台中，对零件破损部位的三维测量是获取再制造模型的关键步骤. 文中提出了一种结构光传感器系统的快速标定方法，对柔性再制造线结构光三维扫描测量系统进行了标定. 标定过程中首先采用平面靶标法标定出CCD 摄像机线性模型的内外参数，然后通过靶标上的结构光条纹的像求解出光平面方程，确定结构光光平面与摄像机的位置关系. 在标定出结构光测量系统的各个参数后，即可以求得零件破损部位特征点的三维坐标，从而获得破损零件的再制造模型. 该方法标定过程简单，精度较高，易于实现现场标定.

关键词：焊接机器人；再制造；结构光；标定
中图分类号：TG115.28 文献标识码：A 文章编号：0253－360X(2009)12－0057－04

0 序 言

零件再制造是一种刚刚兴起的优质、高效、节能、节材的先进制造技术，越来越受到研究者的关注[1－4]. 随着焊接机器人技术和自动控制技术的发展与应用，基于焊接机器人的柔性再制造逐渐成为研究热点. 在基于焊接机器人的柔性再制造平台中，首先要由焊接机器人手臂末端夹持结构光传感器，与变位机协作对破损零件进行三维扫描测量，将测得数据传递给 PC 机，操作者利用这些数据建立零件的再制造模型，再通过机器人控制器控制焊接机器人对零件进行再制造. 可见对零件破损部位的三维测量是获取再制造模型的关键步骤.

目前，结构光法以其大视场、大量程、信息易提取等特点，在三维测量方面得到广泛应用，国内外许多学者对结构光三维测量原理和方法进行了深入研究[5－8].

系统采用结构光三维扫描测量的方法对零件进行测量和建模. 在对零件进行测量之前必须要对系统进行标定，文中采用线结构光扫描的方式对破损零件进行测量，并针对该测量系统的标定问题进行了研究. 系统的标定不仅包括CCD 摄像机的内外参数标定，还包括系统中结构光光平面与摄像机相对位置关系的标定. 标定出结构光测量系统的各个参数后，即可以求得零件破损部位特征点的三维坐标，从而获得破损零件的再制造模型.

收稿日期：2008－08－07
基金项目：国家 863 高技术研究发展计划资助项目(2002AA305402)

1 系统的数学模型

结构光三维测量系统模型如图 1 所示，图 1 中，摄像机为针孔模型，L 为激光发射器与 CCD 摄像机之间的直线距离；f 为摄像机焦距；$O_c x_c y_c z_c$ 为摄像机坐标系，$O_i x_i y_i$ 为像平面坐标系，$O_w X_w Y_w Z_w$ 为世界坐标系；虚线围成的扇面区域为线结构光平面，摄像机主轴 $O_c z_c$ 由 O_c 点出发穿过该平面.

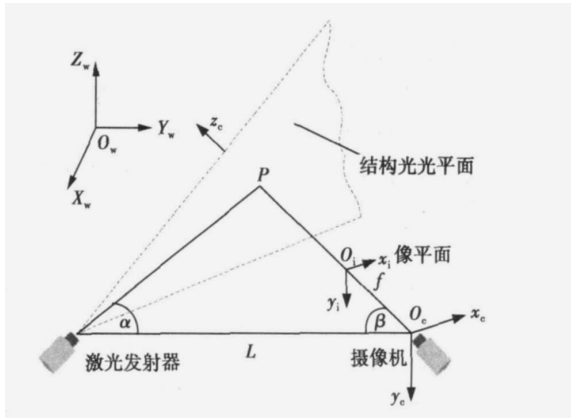

图 1 结构光三维测量系统模型
Fig. 1 Model of structured-light ranging system

假设图 1 中 P 点为代测量物体表面上的一点，则物体目标点 P 在世界坐标系的坐标(X_w, Y_w, Z_w)与其在像平面内的投影点 P' 的坐标(u, v)之间的

关系为[9,10]

$$z_c\begin{bmatrix}u\\v\\1\end{bmatrix}=\begin{bmatrix}\alpha&\gamma&u_0&0\\0&\beta&v_0&0\\0&0&1&0\end{bmatrix}\begin{bmatrix}\boldsymbol{R}&\boldsymbol{t}\\\boldsymbol{0}^{\mathrm{T}}&1\end{bmatrix}\begin{bmatrix}X_w\\Y_w\\Z_w\\1\end{bmatrix}\tag{1}$$

式中: α, β, γ, u_0 为 v_0 为摄像机内部参数; α, β 分别为图像 u 轴和 v 轴上的尺度因子; γ 为描述两图像坐标轴倾斜程度的参数; u_0 和 v_0 为摄像机主点坐标; $\boldsymbol{R}$ 和 $\boldsymbol{t}$ 为摄像机外部参数, 分别表示旋转矩阵和平移矢量. 简记为

$$s\,\tilde{\boldsymbol{m}}=\boldsymbol{K}[\,\boldsymbol{R}\mid\boldsymbol{t}]\,\tilde{\boldsymbol{M}}\tag{2}$$

式中: s 为比例因子; $\tilde{\boldsymbol{M}}$和 $\tilde{\boldsymbol{m}}$分别为齐次矩阵表示的世界坐标和像素坐标; $\boldsymbol{K}=\begin{bmatrix}\alpha&\gamma&u_0\\0&\beta&v_0\\0&0&1\end{bmatrix}$ 为摄像机内部参数矩阵.

结构光光平面方程可由三元一次方程描述为

$$Ax_c+By_c+Cz_c+D=0\tag{3}$$

式中: A, B, C, D 分别为平面方程系数项参数; x_c, y_c, z_c 为光平面上点在摄像机坐标系下的三维坐标. 上述式(2), 式(3)构成了三维扫描测量系统的数学模型.

2 三维扫描测量系统的标定

结构光三维扫描系统的标定主要包括摄像机内外参数的标定和结构光光平面的标定, 即确定结构光光平面与摄像机的位置关系.

2.1 摄像机标定

摄像机的标定是建立从二维图像信息到三维空间信息之间映射的过程. 其标定方法有多种形式, 其中典型的有 Tsai[11] 的两步法, Zhang[12] 提出的基于 2D 平面靶标的标定法和基于 Kruppa 方程的自标定法等[13].

Tsai 方法的高精度需要以设备的高精度为代价, Kruppa 方程的方法在图像序列较长时会不稳定. 作者采用张正友[9] 方法对摄像机进行标定, 该方法使用针孔模型, 但具体标定中结合了自标定法的优点, 其主要思想是假设在标定过程中, 摄像机内部参数保持不变, 只有外部参数发生变化.

假设平面靶标在世界坐标系的 $X_wO_wY_w$ 平面内, 即 $Z_w=0$. 设旋转矩阵 $\boldsymbol{R}$ 的第 i 列为 $\boldsymbol{r}_i$, 从式(2)中可以得到

$$s\begin{bmatrix}u\\v\\1\end{bmatrix}=\boldsymbol{K}[\,\boldsymbol{r}_1\;\boldsymbol{r}_2\;\boldsymbol{r}_3\;\boldsymbol{t}]\begin{bmatrix}X_W\\Y_W\\0\\1\end{bmatrix}=\boldsymbol{K}[\,\boldsymbol{r}_1\;\boldsymbol{r}_2\;\boldsymbol{t}]\begin{bmatrix}X_W\\Y_W\\1\end{bmatrix}\tag{4}$$

由式(4)可知, 靶标平面上的点与其像点之间建立了一个单应性映射, 每一幅图像都可以计算出一个单应性矩阵 $\boldsymbol{H}$, 得

$$s\,\tilde{\boldsymbol{m}}=\boldsymbol{H}\tilde{\boldsymbol{M}},\quad \boldsymbol{H}=\boldsymbol{K}[\,\boldsymbol{r}_1\quad\boldsymbol{r}_2\quad\boldsymbol{t}]\tag{5}$$

令 $\boldsymbol{H}=[\,\boldsymbol{h}_1\quad\boldsymbol{h}_2\quad\boldsymbol{h}_3]$, 由式(5)得

$$[\,\boldsymbol{h}_1\quad\boldsymbol{h}_2\quad\boldsymbol{h}_3]=\lambda\boldsymbol{K}[\,\boldsymbol{r}_1\quad\boldsymbol{r}_2\quad\boldsymbol{t}]$$

式中: λ 为一常数因子. 因为 $\boldsymbol{r}_1$ 和 $\boldsymbol{r}_2$ 是正交单位矢量, 有如下两个约束, 即

$$\boldsymbol{h}_1^{\mathrm{T}}\boldsymbol{K}^{-\mathrm{T}}\boldsymbol{K}^{-1}\boldsymbol{h}_2=0\tag{6}$$

$$\boldsymbol{h}_1^{\mathrm{T}}\boldsymbol{K}^{-\mathrm{T}}\boldsymbol{K}^{-1}\boldsymbol{h}_1=\boldsymbol{h}_2^{\mathrm{T}}\boldsymbol{K}^{-\mathrm{T}}\boldsymbol{K}^{-1}\boldsymbol{h}_2\tag{7}$$

令

$$\boldsymbol{B}=\boldsymbol{K}^{-\mathrm{T}}\boldsymbol{K}^{-1}=\begin{bmatrix}B_{11}&B_{12}&B_{13}\\B_{12}&B_{22}&B_{23}\\B_{13}&B_{23}&B_{33}\end{bmatrix}=$$

$$\begin{bmatrix}\frac{1}{\alpha^2}&-\frac{\gamma}{\alpha^2\beta}&\frac{v_0\gamma-u_0\beta}{\alpha^2\beta}\\-\frac{\gamma}{\alpha^2\beta}&\frac{\gamma^2}{\alpha^2\beta^2}+\frac{1}{\beta^2}&-\frac{\gamma(v_0\gamma-u_0\beta)}{\alpha^2\beta^2}-\frac{v_0}{\beta^2}\\\frac{v_0\gamma-u_0\beta}{\alpha^2\beta}&-\frac{\gamma(v_0\gamma-u_0\beta)}{\alpha^2\beta^2}-\frac{v_0}{\beta^2}&\frac{(v_0\gamma-u_0\beta)^2}{\alpha^2\beta^2}+\frac{v_0^2}{\beta^2}+1\end{bmatrix}\tag{8}$$

注意到 $\boldsymbol{B}$ 是对称的, 定义一个六维矢量为

$$\boldsymbol{b}=[\,B_{11}\quad B_{12}\quad B_{22}\quad B_{13}\quad B_{23}\quad B_{33}]^{\mathrm{T}}$$

令 $\boldsymbol{H}$ 的第 i 列 $\boldsymbol{h}_i=[\,h_{i1}\quad h_{i2}\quad h_{i3}]^{\mathrm{T}}$, 可以得到

$$\boldsymbol{h}_i^{\mathrm{T}}\boldsymbol{B}\boldsymbol{h}_j=\boldsymbol{v}_{ij}^{\mathrm{T}}\boldsymbol{b}\tag{9}$$

式中:

$$\boldsymbol{v}_{ij}=\begin{bmatrix}h_{i1}h_{j1}\\h_{i1}h_{j2}+h_{i2}h_{j1}\\h_{i2}h_{j2}\\h_{i3}h_{j1}+h_{i1}h_{j3}\\h_{i3}h_{j2}+h_{i3}h_{j2}\\h_{i3}h_{j3}\end{bmatrix}$$

则上述由一个给定单应性矩阵所确定的两个摄像机内参数基本约束可重写为

$$\begin{bmatrix}\boldsymbol{v}_{12}^{\mathrm{T}}\\(\boldsymbol{v}_{11}-\boldsymbol{v}_{22})^{\mathrm{T}}\end{bmatrix}\boldsymbol{b}=0\tag{10}$$

如果有平面模板的 n 幅图像, 将上式叠加起来得到 $\boldsymbol{V}\boldsymbol{b}=0$, 其中 $\boldsymbol{V}$ 是一个 $2n\times6$ 的矩阵, 当 $n\geqslant3$ 时, $\boldsymbol{V}^{\mathrm{T}}\boldsymbol{V}$ 最小特征值对应的特征向量就是此方程的解, 求出 $\boldsymbol{b}$ 后, 分解可以得到所有的内参数, 即

$$\left.\begin{aligned} v_0&=(B_{12}B_{13}-B_{11}B_{23})/(B_{11}B_{22}-B_{12}^2)\\ \lambda&=B_{33}-[B_{13}^2+v_0(B_{12}B_{13}-B_{11}B_{23})]/B_{11}\\ \alpha&=\sqrt{\lambda/B_{11}}\\ \beta&=\sqrt{\lambda B_{11}/(B_{11}B_{22}-B_{12}^2)}\\ \gamma&=-B_{12}\alpha^2\beta/\lambda\\ u_0&=\gamma v_0/\beta-B_{13}\alpha^2/\lambda \end{aligned}\right\} \quad (11)$$

从而确定内部参数矩阵 $\boldsymbol{K}$,然后通过式(5)求出外部参数.

2.2　光平面标定

将线结构光投射到靶标平面上,使靶标平面变换 m 个不同的位置($m>2$),提取结构光条纹图像坐标(x_i, y_i). 通过标定的摄像机内外参数,确定靶标平面与摄像机坐标系之间的关系($\boldsymbol{R}$, $\boldsymbol{t}$),根据摄像机针孔模型,即

$$\begin{bmatrix} x_c\\ y_c\\ z_c \end{bmatrix}=\boldsymbol{R}\begin{bmatrix} X_w\\ Y_w\\ Z_w \end{bmatrix}+\begin{bmatrix} t_x\\ t_y\\ t_z \end{bmatrix} \quad (12)$$

代入式(1),并分别计算条纹上点在摄像机坐标系下对应的归一化坐标[x_c, y_c, z_c],从而得到线结构光平面内的点在摄像机坐标系下的坐标,将计算得到的点拟合为一个平面,即

$$Ax_c+By_c+Cz_c+D=0$$

即为光平面方程.

3　试验结果

试验中线结构光三维扫描测量系统由一个单条纹线结构光发射器和一个工业摄像机组成. 在相纸上打印400 mm×400 mm 的棋盘格图案,每个小格为25 mm×25 mm 的正方形,然后把它贴在平整木板上作为靶标,将线结构光条纹投射到靶标上,如图 2 所示. 靶标在摄像机测量空间内自动移动 14 个位置,无需知道运动参数. 利用上述算法求解摄像机内外参数和线结构光光平面方程. 摄像机内部参数标定结果如下. (1) 焦距,(1 284.82, 1 287.78)±(2.54, 2.75). (2) 主点坐标,(366.22, 263.96)±(4.27, 3.86). (3) 畸变系数,(−0.57, 0.96, −0.01, −0.01, 0.00)±(0.01, 0.45, 0.00, 0.00, 0.00). (4) 重投影误差,(0.09, 0.13). 拟合出的光平面方程为

$$0.35x-0.55y+0.64z+0.11=0 \quad (13)$$

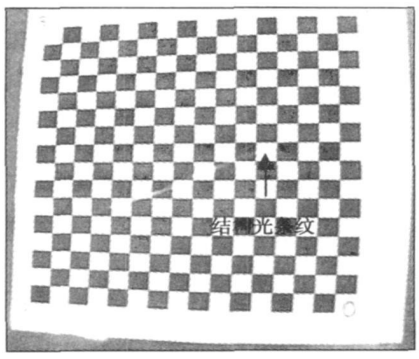

图 2　靶标上的结构光条纹

Fig. 2　structured-light stripe on planar pattern

4　结　　论

(1) 建立了线结构光三维扫描测量系统,该系统由线激光发射器和CCD 摄像机两部分组成. 分两步实现对该系统的快速标定.

(2) 标定过程中平面靶标可以在摄像机测量范围内自由移动,无需知道运动参数,不受人为因素的影响,适于自动化应用.

(3) 文中提出的结构光传感器标定方法操作简单,精度较高.

参考文献:

[1] 徐滨士,张　伟. 现代制造科学之 21 世纪的再制造工程技术及理论研究[C] // 国家自然科学基金委员会机械学科前沿及优先领域研讨论文集. 北京:机械工业出版社,1999:63−67.

[2] Xu Binshi. Nano surface engineering and remanufacturing engineering [J]. Transactions of Nonferrous Metals Society of China, 2004, 14(10): 39−43.

[3] 徐滨士,马世宁,刘世参,等. 绿色再制造工程在军用装备中的应用[J]. 空军工程大学学报(自然科学版),2004,5(1):1−5.
Xu Binshi, Ma Shining, Liu Shican, *et al*. Applications of green remanufacturing engineering to military equipment[J]. Journal of Air Force Engineering University (Natural Science Edition). 2004, 5(1): 1−5.

[4] 崔培枝,姚巨坤,向永华. 柔性再制造体系及其工程应用[J]. 工程机械,2004(2):30−32.
Cui Peizhi, Yao Jukun, Xiang Yonghua. Flexible rebuilding system and its engineering application[J]. Construction Machinery and Equipment, 2004(2): 30−32.

[5] 杜立彬,高晓辉,夏进军,等. 一种新型激光三维扫描测量仪的研制[J]. 激光技术,2005,29(4):366−369.
Du Libin, Gao Xiaohui, Xia Jinjun, *et al*. Research of a novel 3−D laser scanning system [J]. Laser Technology, 2005, 29(4): 366−369.

[6] 何海涛. 复杂面形的光学三维测量相关技术研究[D]. 上海:上海交通大学,2005.

[7] Frank Chen. Overview of three-dimensional shape measurement using optical methods[J]. Optical Engineering, 2000, 39(1): 10—22.

[8] Zonllne F, Matusevich V, Kowarschik R. 3D measurement by stereo-photogrammetry[J]. Proceedings of SPIE, 2003, 5144: 311—314.

[9] 马颂德, 张正友. 计算机视觉—计算机理论与算法基础[M]. 北京: 科学出版社, 1997.

[10] 张广军. 机器视觉[M]. 北京: 科学出版社, 2004.

[11] Tsai R Y. An efficient and accurate camera calibration technique for 3D machine vision[C] // In: Proceedings-CVPR '86: IEEE Computer Society Conference on Computer Vision and Pattern Recognition, Miami Beach, 1986: 364—374.

[12] Zhang Z. A flexible new technique for camera calibration[J]. IEEE Transactions of Pattern Analysis and Machine Intelligence, 2000, 22(11): 1330—1334.

[13] Triggs B. Auto-calibration and absolute quadric[C] // In: Proceedings-CVPR' 97: IEEE Computer Society Conference on Computer Vision and Pattern Recognition, San Juan, 1997: 604—614.

作者简介: 殷子强, 男, 1982 年出生, 博士研究生. 主要从事机器人及智能焊接和焊接机器人再制造方面的研究. 发表论文 2 篇.

Email: mynameisyzq@yahoo.com.cn

[上接第 56 页]

[3] Lei Y P, Murakawa Hidekazu, Shi Y W, *et al*. Numerical analysis of the competitive influence of marangoni flow and evaporation on heat surface temperature and molten pool shape in laser surface remelting [J]. Computational Material Science, 2001, 21(3): 276—290.

[4] Choo R T C, Szedely J. The possible role of turbulence in GTA weld pool behavior[J]. Welding Journal, 1994, 73(2): 25s—31s.

[5] 朱立奎. 基于 FLUENT 横向窄间隙 TIG 焊数值模拟[D]. 北京: 北京工业大学, 2007.

[6] Kim S D, Na S J. Effect of weld pool deformation on weld penetration in stationary gas tungsten arc welding[J]. Welding Journal, 1992, 71(4): 179—193.

[7] 马 立. 等离子弧焊接熔池流场与温度场三维数值模拟[D]. 天津: 天津大学, 2006.

[8] 武传松. 焊接热过程数值分析[M]. 哈尔滨: 哈尔滨工业大学出版社, 1990.

[9] 赵朋成. 全熔透 TIG 焊接池熔池形态瞬时行为的数值模拟[D]. 山东: 山东大学, 2003.

[10] 王献孚, 熊鳌魁. 高等流体力学[M]. 武汉: 华中科技大学出版社, 2003.

作者简介: 袁尤智, 男, 1984 年出生, 硕士研究生. 主要研究方向为光电传感与检测技术. 发表论文 3 篇.

Email: yuanyouzhi1313@sina.com

Key words: TIG welding; weld pool shape; turbulent flow; numerical simulation

Calibration approach for structured-light sensor in remanufacture based on welding robot YIN Ziqiang, ZHANG Guangjun, GAO Hongming, WU Lin (State Key Laboratory of Advanced Welding Production Technology, Harbin Institute of Technology, Harbin 150001, China). p 57—60

Abstract: On the flexible remanufacture platform based on welding robot, 3D ranging of the damage parts is the key step to obtain the remanufacturing data. This paper proposes a rapid calibration approach and calibrates the line structured-light 3D ranging system in the flexible remanufacture platform of the welding robot. The calibration includes the following steps: first, calibrates internal and external parameters of the camera by a planar pattern; second, solves parameters of the light plane by the structured-light strip in the image, which determine the relationship between light plane and camera, and then calculate 3D coordinate of the feature point on the damage parts to establish remanufacture model. The approach is easy, simple and accurate.

Key words: welding robot; remanufacture; structured-light; calibration

Flash butt welding of bainite steel crossing with U71Mn steel rail WANG Xin, ZHANG Fucheng, LÜ Bo, ZHENG Chunlei (State Key Laboratory of Metastable Materials Science and Technology, Yanshan University, Qinhuangdao 066004, China). p 61—64

Abstract: The temperature field distribution of heat-affected zone (HAZ) in weld joints of bainite steel and U71Mn steel and the technical parameters of upset pressure of flash butt welding were determined by using the Gleeble thermal simulation test technology. After some small specimens of bainitic crossing steel and U71Mn rail steel were welded with a miniature flash butt welder by using the results of the parameters to determine the technical parameters of flash butt welding experiment, bainitic steel crossing and U71Mn steel rail were practically welded with Gaas-100 direct current flash butt welder. The mechanical properties, including tensile toughness, impact test and hardness, and the microstructure of welded joints were analyzed. The results show that the best upset pressure of flash butt welding is about 30 MPa, which the HAZ is very small, and the mechanical properties of the welded joint comes up to the standard of the Ministry of Railway. The welding bainitic crossing steel and U71Mn rail steel by flash butt welding is completely feasible.

Key words: crossing; welding; bainite steel

Analysis on the thermal fatigue behavior of QFP soldered joints SHENG Zhong, XUE Songbai, ZHANG Liang, GAO Lili (College of Materials Science and Technology, Nanjing University of Aeronautics and Astronautics, Nanjing 210016, China). p 65—68, 104

Abstract: The creep strain and plastic strain of soldered joints in time history are studied and analyzed with numerical simulation method, which are found to be accumulated as ladder form. Based on Solomon and Shine and Fox models, the fatigue life values of the Sn-Pb and SnAgCu soldered joints are evaluated by equivalent strain, which are about 937 and 1 391 respectively. The experimental results showed both in experiment and simulation results indicate that the tensile force of soldered joints will be decreased with the increase of thermal cycling times, the reliability of SnAgCu after thermal cycling is better than that of Sn-Pb, the fracture mode of the soldered joints transforms from toughness fracture into brittle fracture, and the brittle intermetallic compounds at the interface of soldered joints will grow up gradually with the increase of thermal cycling times during thermal cycling process, which give a strong impact to the reliability of soldered joints and reduce the tensile force of soldered joints at the same time.

Key words: numerical simulation method; fatigue life; tensile force; intermetallic compound

Microstructure of hardfacing metal and matrix materials with high abrasive flux-cored wire LI Da[1], YANG Qingxiang[1], CUI Zhanquan[1], YANG Yulin[2] (1. State Key Laboratory of Metastable Materials Science &Technology, Yanshan University, Qinhuangdao 066004, China; 2. School of Mechanical Engineering, Yanshan University, Qinhuangdao 066004, China). p 69—72

Abstract: Four matrix materials, Y-Ni4 cast iron, 65Mn steel, 40Cr steel and grey cast iron, were hardfaced by the high chromium cast iron of self-shielded flux-cored wire separately. The hardness of different hardfacing specimens was measured, and the microstructures, fracture morphologies and the binding sites of different hardfacing specimens were observed. The results show that the hardness of the hardfacing metal is over 60 HRC and the fracture is of cleavage type. The fusion zones of 65Mn and Y-Ni4 hardfacing metal are good ones. However, the cracks can be observed in the heat-affected zone of Y-Ni4 hardfacing specimen. Therefore, the hardfacing metal of 65Mn steel is suitable for the condition of high stress wear and Y-Ni4 cast iron is suitable for the lower one. Besides, there are many defects in the fusion zone of 40Cr and grey cast iron hardfacing specimens, which are not suitable for the wear resistant matrix materials.

Key words: flux-cored wire; hardfacing metal; binding sites; microstructure

Exploring blowhole resistance of new slag system stainless steel electrode by uniform design method MENG Gongge[1], YANG Deyun[2], LI Dan[1] (1. School of Material Science & Engineering, Harbin University of Science and Technology, Harbin 150040, China; 2. Huade School of Applied Technology, Harbin Institute of Technology, Harbin 150025, China). p 73—76

Abstract: After analyzing some domestic and abroad electrode coating systems, a new slag system of stainless steel electrode was designed. The experiment was arranged by uniform design method and computer program. 11 coating components, each of them being divided into 10 levels, were selected as independent variables, and 30 tests were done in all. The statistical data analysis was done